Peer-reviewed version available at *Appl. Sci.* **2018**, *8*, 610; doi:10.3390/app8040610

Article

Multi-Azimuth Failure Mechanisms in Phosphor-Coated White LEDs by Current Aging Stresses

Zhangbao Peng [1,†], Ziquan Guo [1,†], Tingzhu Wu [1], Peng Zhuang [2], Yuan Shi [2], Tien-Mo Shih [1], Yijun Lu [1], Hao-Chung Kuo [3,4,*] and Zhong Chen [1,*]

1 Department of Electronic Science, Fujian Engineering Research Center for Solid-State Lighting, Xiamen University, Xiamen 361005, China
2 Xiamen Products Quality Supervision & Inspection Institute, National Testing Center for LED Application Products, Xiamen 361004, China
3 Institute of Electro-Optical Engineering, National Chiao Tung University, Hsinchu 30010, Taiwan
4 Department of Electronic Engineering, Xiamen University, Xiamen 361005, China
† These authors contributed equally to this work and should be considered co-first authors
* Correspondence: hckuo@faculty.nctu.edu.tw; chenz@xmu.edu.cn

Abstract: We have experimentally analyzed multi-azimuth degradation mechanisms that govern failures of commercially-available high-power (1 Watt) phosphor-coated white (hppc-W) light-emitting diodes (LEDs) covered with peanut-shaped lenses under three current-stress aging (CSA) conditions. Comprehensive analyses focus on photometric, chromatic, electrical, thermal, and packaging characteristics. At the packaging level, (a) the decrease of the phosphor-conversion efficiency, (b) the yellow-browning of the optical lens, and (c) the darkening of the silver-coated reflective layer deposited with extraneous chemical elements (e.g., C, O, Si, Mg, and Cu, respectively) contribute collectively to the integral degradation of the optical power. By contrast, Ohmic contacts, thermal properties, and angles of maximum intensity remain unchanged after 3840 h aging in three cases. Particularly at the chip level, the formation of point defects increases the number of non-radiative recombination centers, and thus decreases the optical power during aging stages. Nevertheless, in view of the change of the ideality factor, the dopant activation and the annealing effect facilitate the increase of the optical power in two specific aging stages (192 h∼384 h and 768 h∼1536 h), respectively. This work offers a systematic guidance for the development of reliable LED-based light sources in general-lighting areas.

Keywords: light-emitting diodes; failure mechanisms; current-stress aging; reliability

1. Introduction

The solid-state lighting (SSL) technology is regarded as the next-generation lighting approach, and exhibits great advantages of energy-saving, environmental-friendliness, and smart lighting among others [1,2]. It is typically represented by white light-emitting diodes (LEDs), especially for the high-power phosphor-coated white (hppc-W) LEDs, which enjoy additional advantages, such as long lifetime, color-tunable property, and high luminous efficiency [3,4].

However, room for improvements remains, including the internal quantum efficiency of the active region [5,6], the light-extraction technology [7], the current-flow design [8,9], the minimization of resistive loss [10], the electrostatic discharge stability [11], and the color-rendering property via the color mixing [12,13]. Aside these improvements, it is known that, due to their importance, various stress-measured degradation tests, including thermal, electrical, static charges, and moisture, have been developed [14,15]. Generally, these first two are regarded as most commonly-used methods that accelerate the optical degradation [16].

Peer-reviewed version available at Appl. Sci. 2018, 8, 610; doi:10.3390/app8040610

In our study, comprehensive investigations on hppc-WLEDs with peanut-shaped lenses at the chip level and the packaging level under 350 mA, 550 mA, and 750 mA have been conducted. Particularly, peanut-shaped lens offers the optical uniformity and large-view-angle light spatial distributions.

2. Experiments

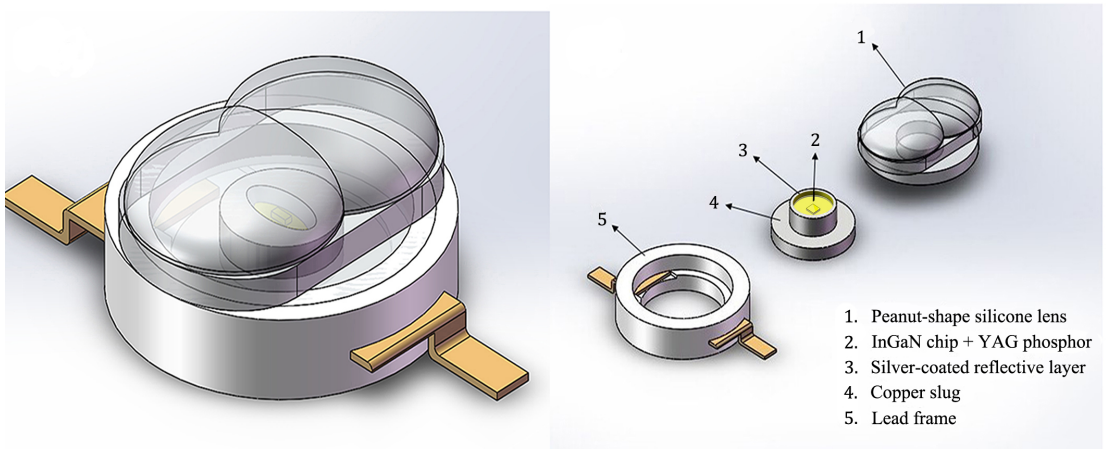

Figure 1. The schematic structure of peanut-shaped hppc-WLEDs.

Each of phosphor-type LEDs consists of a blue InGaN LED chip (with an area of 1 mm × 1 mm), yellow YAG: Ce^{3+} yellow phosphors, a silicone epoxy lens, a silver-coated reflective layer, and other packaging materials, as schematically shown in Figure 1. Three CSA conditions [T = 25 °C, I = 350 mA (CSA-1), T = 25 °C, I = 550 mA (CSA-2), and T = 25 °C, I = 750 mA (CSA-3), respectively] are considered in these experiments. Thirty samples are divided into three groups (each group has 10 samples) corresponding to three stressed conditions. After aging tests, all samples are cooled down in the air for more than 5 h in order to exclude the remaining heat prior to following measurements. The Spectro-320e spectrometer, with a 500 mm integrating sphere (ISP-500, Instrument Systems, Inc.) and an angular distribution analyzer (LEDGON 100, Instrument Systems, Inc.), is employed to measure integral and angular spectral power distributions (SPDs) of these hppc-WLEDs. Therefore, photometric and chromatic analyses can be performed after relevant parameters being obtained from SPDs. Thermal parameters, including the thermal resistance and the junction temperature, can be measured by a transient thermal tester (T3Ster, Micred, Ltd., with an accuracy resolution within 0.1 K). An electric source meter (Keithley-2611, Keithley, Inc.) is used to drive samples, and to measure electrical properties of samples, such as current-voltage (I-V) characteristics and series resistances. The transmittance of silicone lenses and the reflectivity of silver-coated reflective layers are measured by adopting a 150 mm integrating sphere (ISP-150, Instrument Systems, Inc.) with the same spectrometer mentioned above. During measurements, white LEDs are placed on a heat-sink controlled by the temperature controller (Keithley 2510, Keithley, Inc.). In addition, a field emission scanning electron microscopy (FE-SEM, Zeiss Sigma) attached with an energy dispersive spectrometer (EDS, Oxford 7021) is employed to detect and analyze microstructural and compositional changes on surfaces of silver-coated reflective layers before and after aging tests.

3. Results and Discussions

3.1. Photometric and Chromatic Analyses

Figure 2 depicts optical decays of hppc-WLEDs, measured at 350 mA current and the 25 °C heat-sink temperature, for CSA-1, CSA-2, and CSA-3, respectively. As can be observed from Figure 2,

more optical decays occur in the case of CSA-3, indicating that larger current stresses would induce more optical decays during aging. The average optical decays after aging for 3840 h in three cases are 10.2%, 11.0%, and 15.2%, respectively.

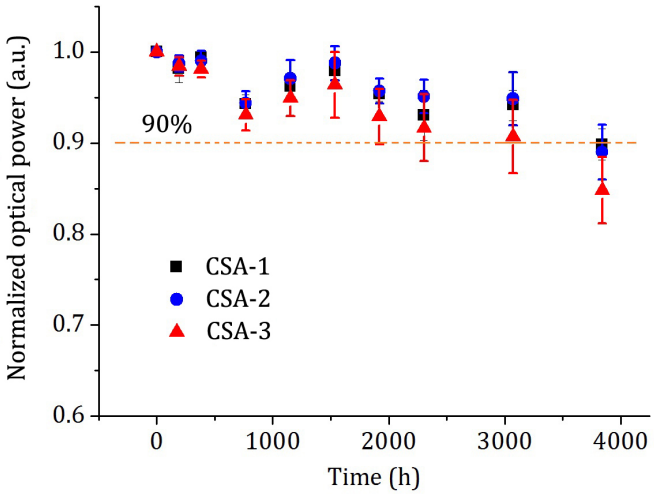

Figure 2. The normalized optical power versus aging time in three cases.

To illustrate the change of correlated color temperature (CCT) [17], we are desired to introduce a parameter, δCCT, which can be written as,

$$\delta CCT = CCT[after] - CCT[before] \quad (1)$$

where $CCT[before]$ and $CCT[after]$ are the CCT value before and after aging, respectively. Figure 3(a) plots the variation of the CCT as a function of time. As can be observed, the CCT value increases as time passes by, but this variation is quite small. After aging for 3840 h, all values of δCCT in three cases are smaller than 200 K. Figures 3(b)∼(d) show measured SPDs in three cases prior to and after aging. Both blue and yellow emissions decrease simultaneously after 3840 h aging. Optical decays of blue and yellow emissions are separately illustrated in these figures. In all three cases, more serious optical degradation can be observed from yellow emissions than blue counterparts. Especially in CSA-3, the optical decay is 12.2% for the blue emission and 17.1% for the yellow emission. To well explain it, we calculate the ratio of the yellow optical power to the blue optical power, namely Y/B=P_{yellow}/P_{blue}, which indirectly describes the phosphor-conversion efficiency (PCE) of hppc-WLEDs [18]. Values of Y/B are also shown in Figures 3(b)∼(d). Changes of Y/B are 2.1%, 4.2%, and 5.6% for CSA-1, CSA-2, and CSA-3, respectively. These changes imply that the PCE slightly decreases after aging, which may be attributed to the wavelength shift of blue LED after 3840 h aging [19]. The higher the aging current is, the more decrease the PCE exhibits. Therefore, we conclude that the PCE decrease during CSA tests is one cause of optical decays for these hppc-WLEDs.

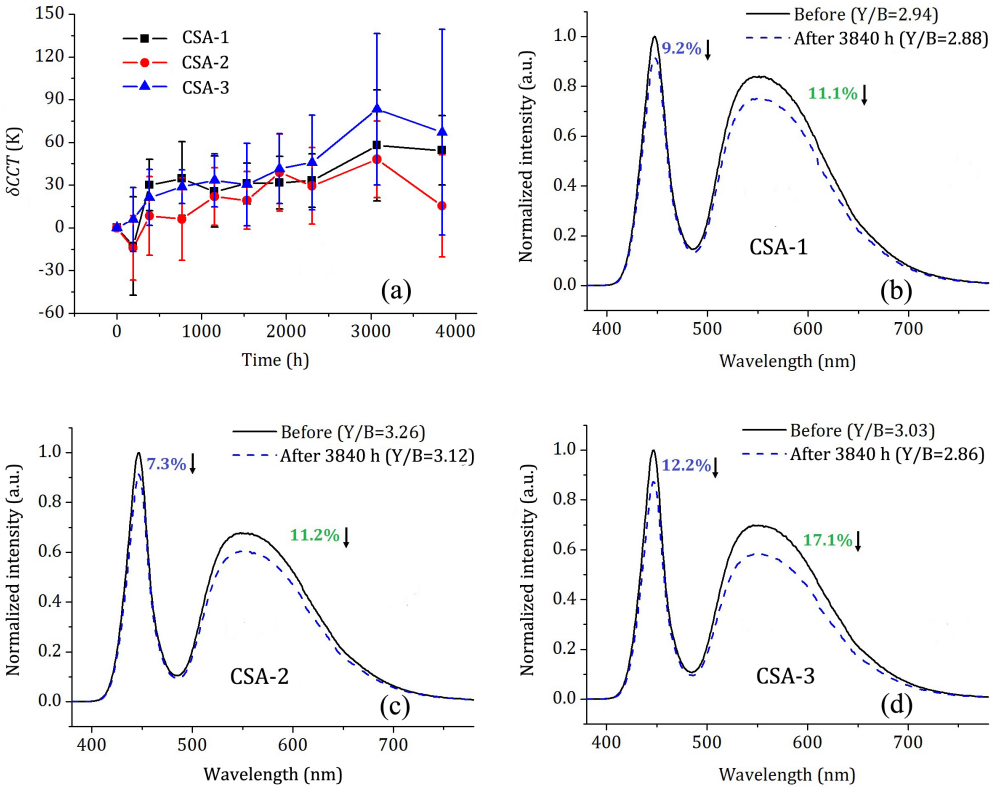

Figure 3. (a) The CCT variation versus time in three cases. SPDs of representative samples for three stresses: (b) CSA-1, (c) CSA-2, and (d) CSA-3, respectively, prior to and after aging.

3.2. Electrical Analyses

Figures 4(a)∼(c) show *I-V* curves of these hppc-WLEDs before and after aging for 3840 h. It is noticed that *I-V* curves of forward voltages larger than 2.5 V are nearly the same before and after stresses in all three cases. This fact attests that indistinct deterioration of Ohmic contacts or/and the active region is observed in all aging stages. However, when the forward voltage is less than 2.5 V, leakage currents at reverse bias and low forward bias are found to increase after stress, which manifests the generation of shunt paths. These shunt paths are acting as non-radiative recombination centers, which root in following mechanisms, such as the generation of nitrogen vacancy and the propagation of non-radiative recombination defects [20,21]. Due to the increase in shunt paths, both the leakage current and the non-radiative recombination center contribute to the decreasing optical power of devices. We also compare optical decays at various currents, which range from 10 mA to 100 mA in three cases. Results, depicted in Figure 4(d), reveal that more distinct optical decays occur at larger currents, opposite to the phenomenon reported in the previous literature [22]. We explain it as, although non-radiative recombination centers in the LED chip may cause more optical decays of blue emissions at smaller currents (seen in [22]), at larger current, optical decays induced by the PCE decrease can lead to more optical decays of total white lights, including both blue and yellow emissions. Because at larger currents, both spectral shifts of the blue emission and the Joule heat accumulation of LED devices are more prominent during the operation, resulting in more PCE decreases.

Preprints (www.preprints.org) | NOT PEER-REVIEWED | Posted: 15 March 2018 doi:10.20944/preprints201803.0123.v1

Peer-reviewed version available at Appl. Sci. 2018, 8, 610; doi:10.3390/app8040610

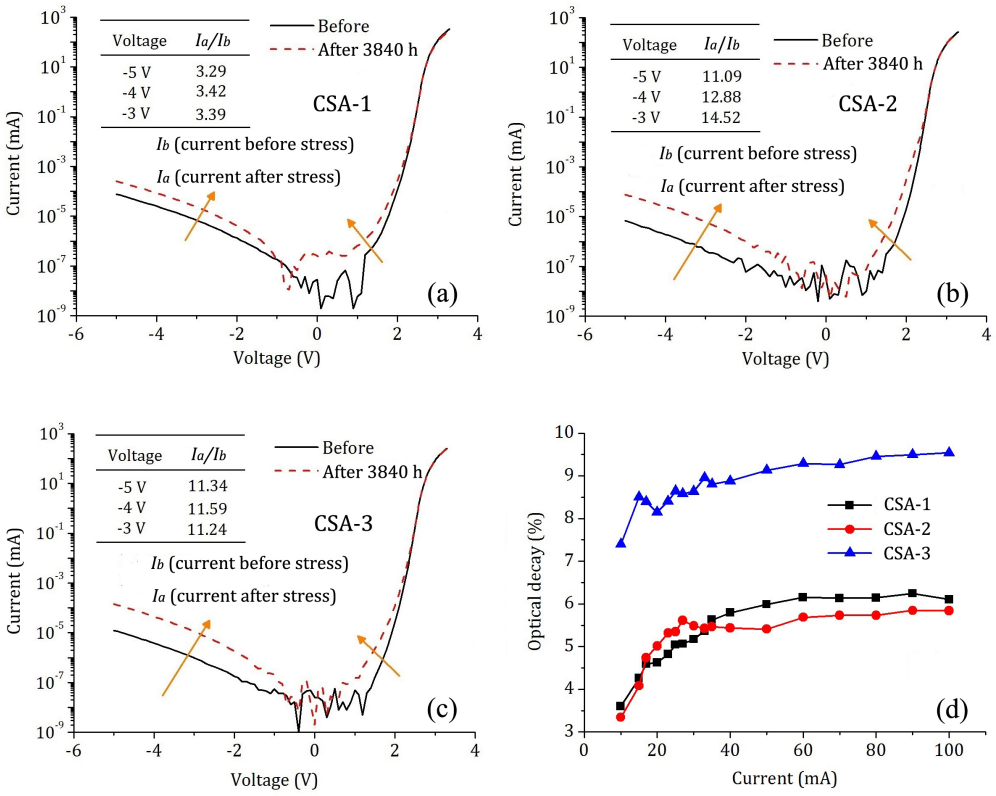

Figure 4. The *I-V* curves of representative hppc-WLEDs before and after 3840 h aging in cases of (a) CSA-1, (b) CSA-2, and (c) CSA-3, respectively. (d) Optical decays at various currents in three cases.

Figure 5 shows forward voltages of representative hppc-WLEDs prior to and after aging tests. Forward voltages and series resistances (according to the equation in the inset in Figure 5, where V_f is the forward voltage, h is the Planck constant, hv is the photon energy, e is the elementary charge, R_s is the series resistance, and I is the electrical current) remain the same during aging periods in three cases, indicating again that Ohmic contacts or/and the active region remain unchanged after aging.

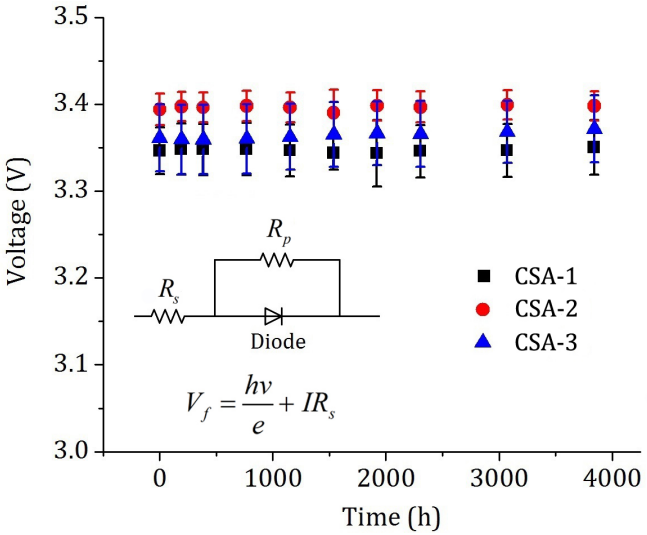

Figure 5. Forward voltages of representative hppc-WLEDs during 3840 h aging in three cases.

Peer-reviewed version available at Appl. Sci. 2018, 8, 610; doi:10.3390/app8040610

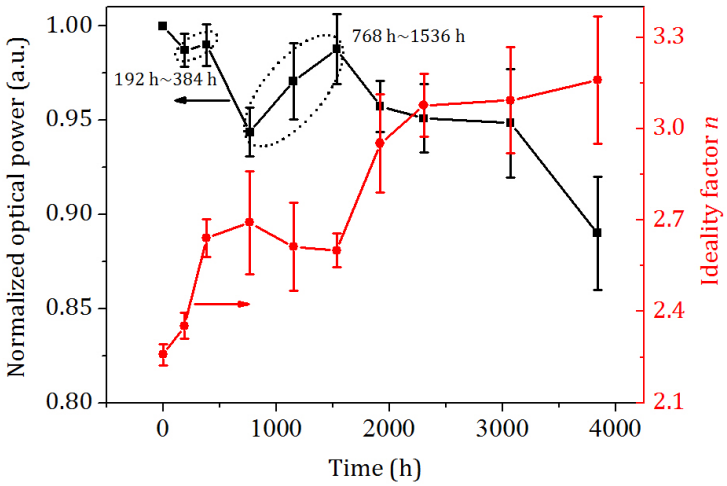

Figure 6. For the case of CSA-2 measured at 350 mA: the normalized optical power versus aging time (black square, left vertical axis) and the ideality factor versus aging time (red circle, right vertical axis) with error bars.

To further study degradation mechanisms in chips from *I-V* characteristics, we selected the result of devices in CSA-2 as an example (similar results can be found in CSA-1 and CSA-3). Figure 6 illustrates the degradation of the optical power in the case of CSA-2 (black square), and the corresponding change of the ideality factor n (red circle) which is calculated via the *I-V* curve fitting by using the Sah-Noyce-Shockley model [23]. As can be noticed, the optical power keeps decreasing in all aging stages except in two specific periods (192 h∼384 h and 768 h∼1536 h), whereas the ideality factor performs an inverse evolution in these stages except in the period (768 h∼1536 h). On this occasion, it is plausible to associate a relationship between the optical power and the ideality factor. That is, the decrease in optical power is generally related to the increase in ideality factor. In general, point defects, such as nitrogen vacancies and gallium vacancies, assist electrons tunneling into quantum wells [24]. As a consequence, the ideality factor poses an increase as the optical power experiences a decrease, due to the generation of point defects. However, in the first specific period (192 h∼384 h), the optical power turns to increase slightly and the ideality factor increases too. We attribute this abnormal change to the dopant activation, because of the improvement of the effective carrier concentration reactivated by Mg-H complexes in the p-GaN [25]. In the second specific period (768 h∼1536 h), the optical power turns to increase but the ideality factor starts to decrease inversely. This opposite change can be assigned to the annealing effect [26], which wipes out partial defects after being subjected to the long-term high-current stress. Therefore, the annealing effect dominates the second specific period and thus leads to the decrease in the ideality factor as well as the increase in the optical power.

3.3. Thermal Analyses

We also perform thermal analyses on these hppc-WLEDs. Thermal resistances of samples are measured by the transient thermal tester. Based on the cumulative structure function by T3Ster software, plotted in Figure 7(a), we can discern different thermal resistances in components of the LED, including the die, the die attach, the silver adhesive, and the copper, respectively. Figures 7(b)∼(d) show cumulative structure functions of hppc-WLEDs before stress and after aging for 3840 h in three cases. Compared with respective initial values of thermal resistances, it is found that only small alterations ($\delta(R_{th})$ is less than 1 K/W) can be observed, indicating that the thermal property remains unchanged in three cases during aging stages.

Preprints (www.preprints.org) | NOT PEER-REVIEWED | Posted: 15 March 2018 doi:10.20944/preprints201803.0123.v1

Peer-reviewed version available at Appl. Sci. 2018, 8, 610; doi:10.3390/app8040610

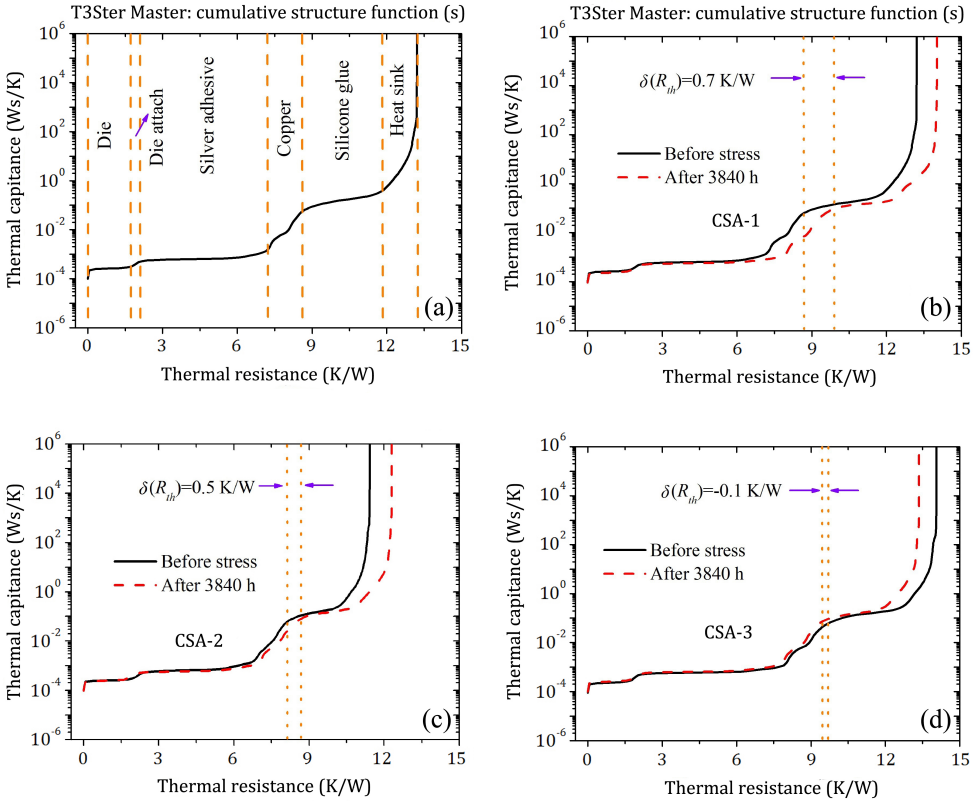

Figure 7. (a) The cumulative structure function of samples, and those of samples before and after 3840 h aging in cases of (b) CSA-1, (c) CSA-2, and (d) CSA-3, respectively.

3.4. Packaging Analyses

Figure 8(a) depicts the photograph of four representative samples corresponding to before and after aging for 3840 h. The sample number of analyzed samples are #6 (CSA-1), #16 (CSA-2), and #23 (CSA-3), respectively. The ratio of the optical power after 3840 h aging to the optical power before stress for #6, #16, and #23 are 90.8%, 90.2%, and 80.7%, respectively, corresponding to 9.2%, 9.8%, and 19.3% optical decay, respectively. From the appearance in Figure 8(a), the sample of CSA-2 exhibits remarkable yellow-browning in the optical lens, whereas the sample of CSA-3 demonstrates distinct darkening in the silver-coated reflective layer. Considering the optical decay and the surficial change, we deduce that darkening in the silver-coated reflective layer produces more serious degradation of the optical power than yellow-browning in the silicone-based optical lens does.

Additionally, the angular intensity distribution with respect to four samples (one unaged sample and three aged ones) is shown in Figure 8(b), where luminous intensity distributions are of the batwing type for peanut-shaped LEDs with maximum intensities at $\pm$ 60°. Large view angle in these peanut-shaped LEDs is quite different from that in hemisphere-shaped LEDs [27]. Compared with the unaged sample, angles of the maximum intensity remain constant, whereas aged ones in three cases demonstrate continuous decreases in intensity at all tested angles as the current stress increases. These decreases may be attributed to the degradation of all components in hppc-WLEDs, such as the yellow-browning of optical lens, the darkening of silver-coated reflective layer, and the decomposition of phosphor-silicone mixtures.

Peer-reviewed version available at Appl. Sci. 2018, 8, 610; doi:10.3390/app8040610

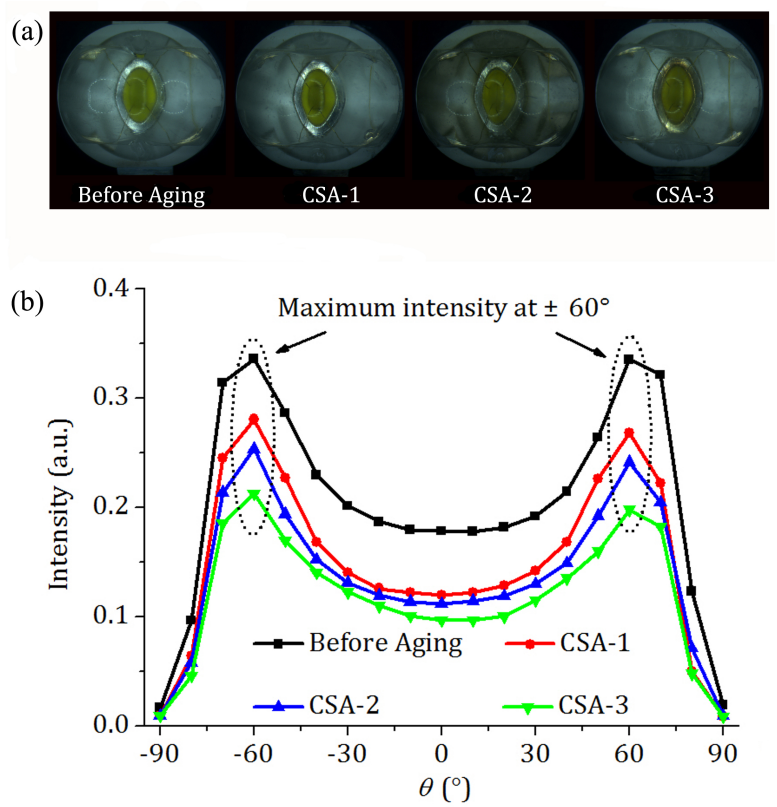

Figure 8. (a) The photographs of four representative samples, and (b) angular intensity distributions for these hppc-WLEDs.

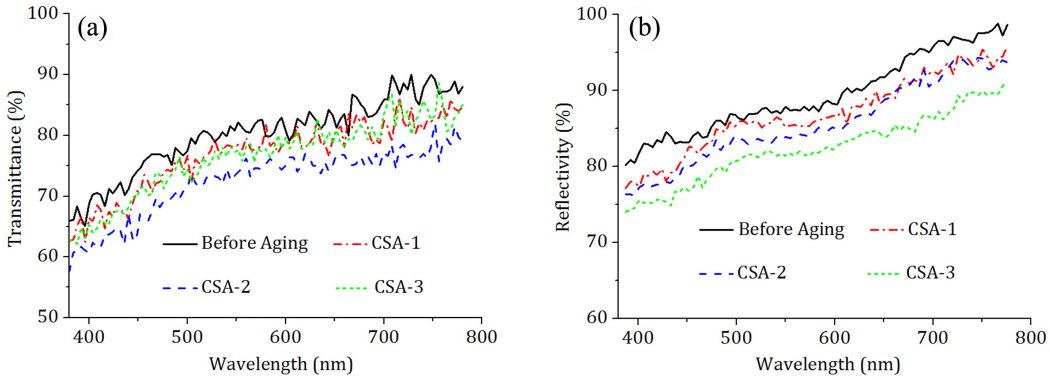

Figure 9. (a) The transmittance of an unaged silicone lens (before aging), and of three lenses after aging in CSA-1, CSA-2, and CSA-3, respectively. (b) The reflectivity of silver-coated reflective layers before and after aging in CSA-1, CSA-2, and CSA-3, respectively.

We employ a white LED (with the current driven at 350 mA and the heat-sink temperature maintained at 25 °C) to measure and compare the transmittance of silicone lenses and the reflectivity of silver-coated reflective layers in an unaged device and three 3840 h-aged devices in CSA-1, CSA-2, and CSA-3, respectively. As shown in Figure 9(a), all transmittances of aged lenses experience a decrease in comparison to the unaged one at measured wavelengths between 380 nm and 780 nm. However, it is obvious to distinguish that the transmittance of the lens in CSA-2 drops the most seriously than that of lenses in other cases. The reason for this loss lies in that the device in CSA-2 exhibits a prominent yellow-browning silicone lens. Besides, variations of reflectivity with respect to silver-coated reflective

Peer-reviewed version available at Appl. Sci. 2018, 8, 610; doi:10.3390/app8040610

layers before and after aging are shown in Figure 9(b). The optical reflectivity in CSA-3 is generally less than that in CSA-1 and CSA-2 in the visible wavelength range, which can be greatly attributed to the darkening of the silver-coated reflective layer. Therefore, both the descending transmittance of the silicone lens and the declining reflectivity of the silver-coated reflective layer are found to be strongly related to the decay of optical power after aging.

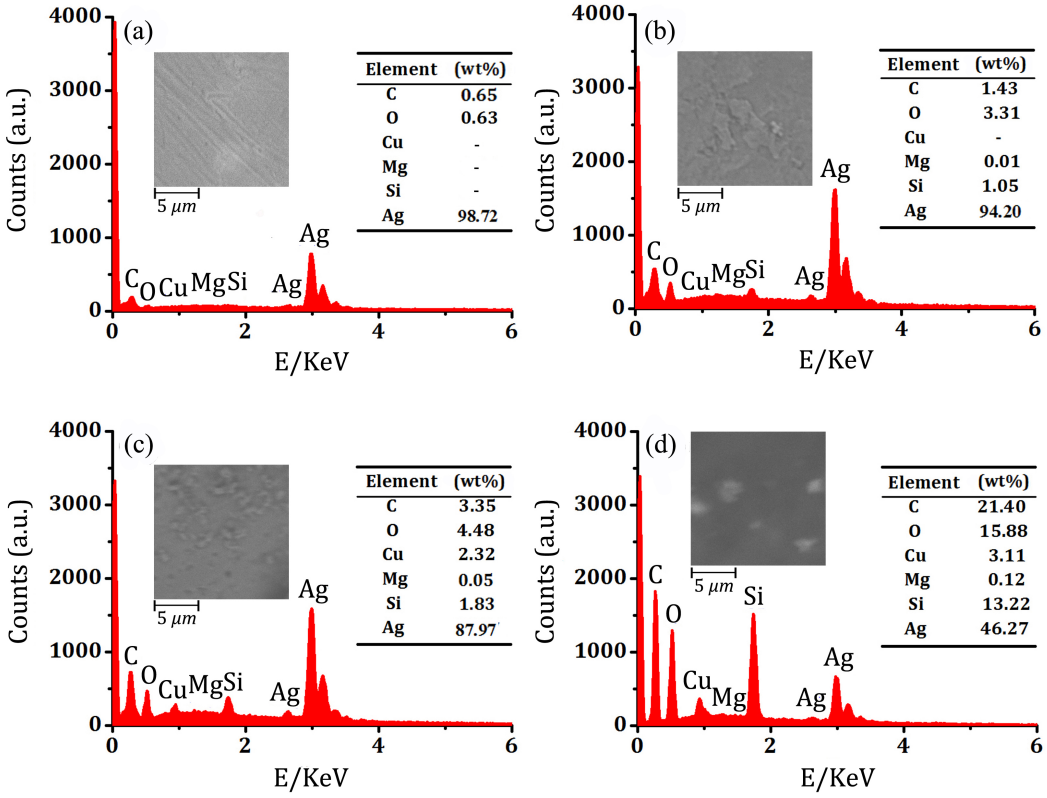

Figure 10. The SEM micrographs and the chemical element content on the surfaces of silver reflective layers by EDS: (a) one untreated sample (before aging), and three representative stressed samples in (b) CSA-1, (c) CSA-2, and (d) CSA-3, respectively (after 3840 h aging).

To further investigate the degradation of silver reflective layers, we employed a FE-SEM attached with an EDS on surfaces of silver-coated reflective layers to observe their microstructural and compositional changes after 3840 h aging, as shown in Figure 10. Results indicate that, compared with the untreated sample [Figure 10(a)], surfaces of aged silver-coated reflective layers generate dark areas and extra chemical elements to varying degrees [Figures 10(b)∼((d)]. In detail, the increase of elements C and O, the most significant factors for the degradation of the optical power, can be assigned to the carbonization behavior on the surface of silver-coated reflective layers [28]. Especially in CSA-3, the element C increases from 0.65 wt% to 21.40 wt%, and in the meantime, the element O is up to 15.88 wt% from 0.63 wt%. The element Si with 13.22 wt% in CSA-3 is much higher than that with only 1.05 wt% in CSA-1 and 1.83 wt% in CSA-2. We suppose that most of the element Si may deposit from phosphor-silicone mixtures when they are subjected to the high-current stress. In addition, small amounts of the element Cu (CSA-1: none, CSA-2: 2.32 wt%, CSA-3: 3.11 wt%) and Mg (CSA-1: 0.01 wt%, CSA-2: 0.05 wt%, CSA-3: 0.12 wt%) emerge on surfaces of aged silver-coated reflective layers. It is conceivable to deduce that both elements Cu and Mg are highly correlated with the high-current stress. Furthermore, the former element may stem from the copper slug, and meanwhile the latter one is considered to be imported from the reactivation of Mg-H complexes in p-GaN [29].

4. Conclusion

We have investigated multiple degradation mechanisms of hppc-WLEDs under three current stresses (CSA-1, CSA-2, and CSA-3, respectively), with major findings listed below. 1) During aging, both blue and yellow parts of spectra in hppc-WLEDs are dwarfed in three cases. Via the calculation of Y/B ratios, the decrease of phosphor-conversion efficiency after current stresses has been indirectly observed. This fact adequately supports the explanation for the relationship between optical decay at different currents. 2) Increases in leakage currents at reverse bias and low forward bias (when the forward voltage is smaller than 2.5 V) after stresses indicate that the generation of shunt paths is attributed to the optical decay of samples. 3) Due to the increase in point defects, optical powers exhibit a decrease during aging stages. By contrast, the reactivation of Mg-H complexes and the annealing effect are respectively responsible for the optical power increase in two aging periods (192 h∼384 h and 768 h∼1536 h). 4) Ohmic contacts and thermal resistances remain unchanged during aging tests. 5) Large view angles located in peanut-shaped hppc-WLEDs manifest a batwing-type angular emission distribution, whereas intensities at all tested angles continue to decline as the current stress increases due to the degradation of all components in LEDs. 6) The darkening of silver-coated reflective layers caused primarily by the carbonization behavior contributes more greatly to the optical decay of samples than the yellow-browning of optics lens does. Therefore, in this study, we have presented a comprehensive description of the photometric, chromatic, electrical, thermal, and packaging analyses of hppc-WLEDs in current-stress aging processes. In real applications, these experimental conclusions can provide an applicable guidance to develop reliable LED-based light sources.

Acknowledgments: This work was supported in parts by the International Science and Technology Cooperation Program of China (2015DFG62190), the Hong Kong, Macao, and Taiwan Special Science and Technology Cooperation Program (2015DFT10120), the National Natural Science Foundation of China (61504112, 11604285, and 51605404), the Technological Innovation Project of Economic and Information Commission of Fujian Province, and the Strait Postdoctoral Foundation of Fujian Province.

Author Contributions: Hao-Chung Kuo and Zhong Chen proposed the main idea; Zhangbao Peng and Ziquan Guo performed all experiments and wrote the manuscript; Tingzhu Wu and Peng Zhuang analyzed the data; Yuan Shi, Tien-Mo Shih, and Yijun Lu have contributed to the final revision.

Conflicts of Interest: The authors declare no conflict of interest.

References

1. Schubert, E. F.; Kim, J. K. Solid-state light sources getting smart. *Science* **2005**, *308*, 1274-1278; DOI:10.1126/science.1108712.
2. Crawford, M. H. LEDs for solid-state lighting: performance challenges and recent advances. *IEEE J. Sel. Top. Quantum Electron.* **2009**, *15*, 1028-1040; DOI:10.1109/JSTQE.2009.2013476.
3. Lin, H. Y.; Chen, K. J.; Wang, S. W.; Lin, C. C.; Wang, K. Y.; Li, J. R.; Lee, P. T.; Shih, M. H.; Li, X. L.; Chen, H. M.; Kuo, H. C. Improvement of light quality by DBR structure in white LED. *Opt. Express* **2015**, *23*, 27-33; DOI:10.1364/OE.23.000A27.
4. Guo, Z. Q.; Shih, T. M.; Lu, Y. J.; Gao, Y. L.; Zhu, L. H.; Chen, G. L.; Zhang, J. H.; Lin, S. Q.; Chen, Z. Studies of scotopic/photopic ratios for color-tunable white light-emitting diodes. *IEEE Photon. J.* **2013**, *5*, 8200409; DOI:10.1109/JPHOT.2013.2273736.
5. Kim, G.; Sun, M. C.; Kim, J. H.; Park, E.; Park, B. G. GaN-based light emitting diodes using p-type trench structure for improving internal quantum efficiency. *Appl. Phys. Lett.* **2017**, *110*, 021115; DOI:10.1063/1.4973995.
6. Tsai, Y. L.; Liu, C. Y.; Krishnan, C.; Lin, D. W.; Chu, Y. C.; Chen, T. P.; Shen, T. L.; Kao, T. S.; Charlton, M. D. B.; Yu. P.; Lin, C. C.; Kuo, H. C.; He, J. H. Bridging the "green gap" of LEDs: giant light output enhancement and directional control of LEDs via embedded nano-void photonic crystals. *Nanoscale* **2016**, *8*, 1192-1199; DOI:10.1039/c5nr05555e.
7. Fadil, A.; Ou, Y. Y.; Iida, D.; Kamiyama, S.; Petersen, P. M.; Ou, H. Y. Combining surface plasmonic and light extraction enhancement on InGaN quantum-well light-emitters. *Nanoscale* **2016**, *8*, 16340-16348; DOI:10.1039/C6NR04375E.

8. Hao, G. D.; Taniguchi, M.; Tamari, N.; Inoue, S. Enhanced wall-plug efficiency in AlGaN-based deep-ultraviolet light-emitting diodes with uniform current spreading p-electrode structures. *J. Phys. D: Appl. Phys.* **2016**, *49*, 1-8; DOI:10.1088/0022-3727/49/23/235101.
9. Wu, P. C.; Ou, S. L.; Horng, R. H.; Wuu, D. S. Improved performance of high-voltage vertical GaN LEDs via modification of micro-cell geometry. *Appl. Sci.* **2017**, *7*, 506; DOI:10.3390/app7060506.
10. Kim, T.; Seong, T. Y.; Kwon, O. Investigating the origin of efficiency droop by profiling the voltage across the multi-quantum well of an operating light-emitting diode. *Appl. Phys. Lett.* **2017**, *108*, 231101; DOI:10.1063/1.4953401.
11. Chen, S. L. Enhanced electrostatic discharge reliability in GaN-based light-emitting diodes by the electrode engineering. *J. Disp. Technol.* **2014**, *10*, 779-785; DOI:10.1109/JDT.2014.2321460.
12. Guo, Z. Q.; Shih, T. M.; Gao, Y. L.; Lu, Y. J.; Zhu, L. H.; Chen, G. L.; Lin, Y.; Zhang, J. H.; Chen, Z. Optimization studies of two-phosphor-coated white light-emitting diodes. *IEEE Photon. J.* **2013**, *5*, 8200112; DOI:10.1109/JPHOT.2013.2245885.
13. Shen, W. Q.; Zhu, Y. W.; Wang, Z. L. Luminescent properties of $Sr_4Si_3O_8Cl_4$:Eu^{2+}, Bi^{3+} phosphors for near UV InGaN-based light-emitting-diodes. *Appl. Sci.* **2015**, *5*, 1494-1502; DOI:10.3390/app5041494
14. Meneghini, M.; Lago, M. D.; Trivellin, N.; Meneghesso, G.; Zanoni, E. Degradation mechanisms of high-power LEDs for lighting applications: an overview. *IEEE Trans. Ind. Appl.* **2014**, *50*, 78-85; DOI:10.1109/TIA.2013.2268049.
15. Liu, L. L.; Ling, M. J.; Yang, J. F.; Xiong, W.; Jia, W. Q.; Wang, G. Efficiency degradation behaviors of current/thermal co-stressed GaN-based blue light emitting diodes with vertical-structure. *J. Appl. Phys.* **2012**, *111*, 093110; DOI:10.1063/1.4712030.
16. Lago, M. D.; Meneghini, M.; Trivellin, N.; Zanoni, M. E. Degradation mechanisms of high-power white LEDs activated by current and temperature. *Microelectron. Reliab.* **2011**, *51*, 1742-1746; DOI:10.1016/j.microrel.2011.06.057.
17. Chen, H. T.; Hui, S. Y. Dynamic prediction of correlated color temperature and color rendering index of phosphor-coated white light-emitting diodes. *IEEE Tran. Ind. Electron.* **2014**, *61*, 784-797; DOI:10.1109/TIE.2013.2251736.
18. Yang, T. H.; Wu, S. M.; Sun, C. C.; Glorieux, B.; Chen, C. Y.; Chang, Y. Y.; Lee, X. H.; Yu, Y. W.; Chung, T. Y.; Lai, K. Y. Stabilizing CCT in pcW-LEDs by self-compensation between excitation efficiency and conversion efficiency of phosphors. *Opt. Express* **2017**, *25*, 29287-29295; DOI:10.1364/OE.25.029287.
19. Fu, H. K.; Lin, C. W.; Chen, T. T.; Chen, C. L.; Chou, P. T.; Sun, C. J. Investigation of dynamic color deviation mechanisms of high power light-emitting diode. *Microelectron. Reliab.* **2012**, *52*, 866-871; DOI:10.1016/j.microrel.2011.04.025.
20. Kang, B.; Kim, S. B. Temperature dependence of the component currents and internal quantum efficiency in blue light-emitting diodes. *IEEE Trans. Electron Dev.* **2013**, *60*, 1060-1067; DOI:10.1109/TED.2013.2242470.
21. Han, D. P.; Kim, Y. J.; Shim, J. I.; Shin, D. S. Forward-capacitance measurement on wide-bandgap light-emitting diodes. *IEEE Photon. Tech. Lett.* **2016**, *28*, 2407-2410; DOI:10.1109/LPT.2016.2597158.
22. Meneghini, M.; Tazzoli, A.; Mura, G.; Meneghesso, G.; Zanoni, E. A review on the physical mechanisms that limit the reliability of GaN based LEDs. *IEEE Trans. Electron Dev.* **2010**, *57*, 108-118; DOI:10.1109/TED.2009.2033649.
23. Spencer, P.; Clarke, E.; Murray, R. Carrier escape and the ideality factor in quantum dot p-n junctions. *IEEE J. Quantum Elect.* **2014**, *50*, 213-219; DOI:10.1109/JQE.2014.2303515.
24. Monti, D.; Meneghini, M.; Santi, C. D.; Meneghesso, G.; Zanoni, E. Degradation of UVA LEDs: physical origin and dependence on stress conditions. *IEEE Trans. Device Mater. Rel.* **2016**, *16*, 213-218; DOI:10.1109/TDMR.2016.2558473.
25. Su, C. Y.; Tu, C. G.; Liu, W. H.; Lin, C. H.; Yao, Y. F.; Chen, H. T.; Wu, Y. R.; Kiang, Y. W.; Yang, C. C. Enhancing the hole-injection efficiency of a light-emitting diode by increasing Mg doping in the p-AlGaN electron-blocking layer. *IEEE Trans. Electron Dev.* **2017**, *64*, 3226-3233; DOI:10.1109/TED.2017.2711023.
26. Chen, T. T.; Wang, C. P.; Fu, H. K.; Chou, P. T.; Ying, S. P. Electroluminescence enhancement in InGaN light-emitting diode during the electrical stressing process. *Opt. Express* **2014**, *22*, 1328-1333; DOI:10.1364/OE.22.0A1328.

27. Wang, K.; Wu, D.; Chen, F.; Liu, Z. Y.; Luo, X. B.; Liu, S. Angular color uniformity enhancement of white light-emitting diodes integrated with freeform lenses. *Opt. Lett.* **2010**, *35*, 1860-1862; DOI:10.1364/OL.35.001860.
28. Tsai, M. Y.; Tang, C. Y.; Wang, C. H.; Tsai, Y. Y.; Chen, C. H. Investigation on some parameters affecting optical degradation of LED packages during high-temperature aging. *IEEE Trans. Device Mater. Rel.* **2015**, *15*, 335-341; DOI:10.1109/TDMR.2015.2441751.
29. Lu, Y. J.; Guo, Z. Q.; Shih, T. M.; Gao, Y. L.; Huang, W. L.; Lu, H. L.; Lin, Y.; Chen, Z. Optical degradation mechanisms of indium gallium nitride-based white light emitting diodes by high-temperature aging tests. *IEEE Trans. Rel.* **2016**, *65*, 256-262; DOI:10.1109/TR.2015.2444834.